A Finite-Difference Framework for Saint-Venant Torsion of Axisymmetric Shafts with Variable Diameter

Javlonbek Turdibekov[1, a)] and Farkhadjan Adilov[1, b)]

[1]*Institute of Mechanics and Seismic Stability of Structures named after M.T. Urazbaev, Uzbekistan Academy of Sciences, Tashkent, Uzbekistan*

[a)]Corresponding author: javlonbek.turdibekov9@gmail.com
[b)]mahzun86@gmail.com

Abstract. We develop and document a robust finite-difference (FDM) solver for the Saint-Venant torsion of circular, axially variable-diameter shafts $r = R(z)$. The formulation is based on the Prandtl stress function, mapped to a rectangular computational domain via $r = \rho R(z)$ with $\rho \in [0,1]$ and $z \in [0, L]$. The resulting elliptic PDE has variable coefficients and a weak mixed derivative; we discretize it with second-order central differences (and, as an alternative, Chebyshev collocation in ρ) and solve with Successive Over-Relaxation (SOR) or Krylov methods. Both twist-controlled and torque-controlled load cases are treated consistently through an axis condition on the stress function. We report implementation details, convergence checks, and verification against the classical constant-radius solution. The method produces stress distributions $\tau_{r\theta}, \tau_{z\theta}$ and the torque profile $T(z)$; it is immediately extensible to temperature-dependent shear modulus $G(T)$ and eigen-twist sources driven by thermal gradients. This capability is relevant to design and life assessment of power-train shafts, rotors, turbine spindles, and process-industry rolls where diameter tapers or turned shoulders are common.

INTRODUCTION

Torsion of nonuniform circular shafts arises in numerous engineered systems: automotive and aerospace drive shafts with tapered sections, compressor/turbine rotors, line-shafting with bearing seats and fillets, and paper/steel mill rolls. Saint-Venant's theory remains the workhorse for elastic torsion where warping is restrained only by free lateral surfaces. Using the Prandtl stress function reduces the equilibrium equations to a scalar elliptic PDE and provides direct access to shear stresses and torque. When the radius varies along the axis, $R(z)$, the physical domain is no longer cylindrical and a practical numerical treatment benefits from a mapping to a rectangle. This paper presents a compact, production-ready FDM formulation on (ρ, z) grids, including mixed-derivative treatment, boundary/load control, and diagnostics for accuracy. For higher spectral accuracy across the radius, we also outline a Chebyshev collocation variant in ρ[1].

MATERIALS, METHODS, AND OBJECT OF STUDY

The object of study is an axisymmetric circular rod (tapered shaft) made of an isotropic elastic material. The radius varies linearly along its length, forming a truncated cone geometry. The analysis assumes axisymmetric torsion with the only nonzero displacement component being the circumferential one (r,).

The material shear modulus G is considered both constant and variable along the longitudinal coordinate to model thermal or compositional gradients. The effect of temperature is incorporated through a temperature-dependent modulus (z,)=G_0[1−αT(T(z)−T_0)], allowing comparison between purely mechanical and thermomechanically coupled torsion cases[2].

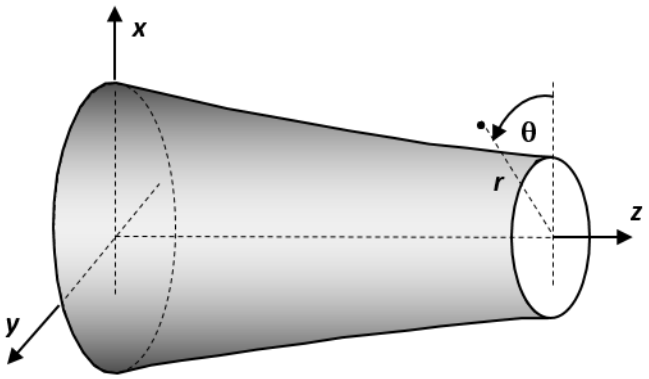

FIGURE 1. Axisymmetric circular shaft with variable diameter

Displacement assumption. For axisymmetric torsion we take only a circumferential displacement,

$$u_\theta = u_\theta(r,z), \qquad u_r = 0, \quad u_z = 0, \tag{1}$$

u and all fields are independent of $(\partial(\ )/\partial\theta = 0)$.

Small-strain components in cylindrical coordinates. The engineering shear strains that involve u_θ are:

$$\gamma_{r\theta} = \frac{\partial u_\theta}{\partial r} - \frac{u_\theta}{r}, \quad \gamma_{z\theta} = \frac{\partial u_\theta}{\partial z}. \tag{2}$$

Derivation sketch. Starting from the small-strain tensor $\varepsilon_{ij} = \frac{1}{2}\left(u_{i,j} + u_{j,i}\right)$ in cylindrical coordinates, the nonzero metric coefficients give [3]:

$$\varepsilon_{r\theta} = \frac{1}{2}\left(\frac{1}{r}\frac{\partial u_r}{\partial \theta} + \frac{\partial u_\theta}{\partial r} - \frac{u_\theta}{r}\right), \qquad \varepsilon_{z\theta} = \frac{1}{2}\left(\frac{\partial u_\theta}{\partial z} + \frac{1}{r}\frac{\partial u_z}{\partial \theta}\right). \tag{3}$$

With axisymmetry $(\partial(\ )/\partial\theta = 0)$ and $u_r = u_z = 0$, the engineering (tensor-double) shears are

$$\gamma_{r\theta} = 2\varepsilon_{r\theta} = \partial u_\theta/\partial r - u_\theta/r \qquad \text{and} \qquad \gamma_{z\theta} = 2\varepsilon_{z\theta} = \partial u_\theta/\partial z.$$

For isotropic linear elasticity the shear stresses are proportional to the shear strains via the shear modulus G:

$$\tau_{r\theta} = G\gamma_{r\theta}, \qquad \tau_{z\theta} = G\gamma_{z\theta}. \tag{4}$$

(If desired, G may be treated as constant in the baseline model or allowed to vary with temperature $G(T)$ in extensions.)

Neglecting body forces, the divergence of the Cauchy stress must vanish. The θ-component of ∇σ=0 in cylindrical coordinates is

$$\frac{1}{r}\frac{\partial}{\partial r}\left(r\sigma_{r\theta}\right) + \frac{1}{r}\frac{\partial \sigma_{\theta\theta}}{\partial \theta} + \frac{\partial \sigma_{z\theta}}{\partial z} = 0. \tag{5}$$

Under axisymmetry $(\partial(\ )/\partial\theta = 0)$. and since torsion produces no $\sigma_{\theta\theta}$ contribution in Saint-Venant theory, we obtain the scalar equilibrium equation for shear:

$$\frac{1}{r}\frac{\partial}{\partial r}\left(r\tau_{r\theta}\right) + \frac{\partial \tau_{z\theta}}{\partial z} = 0. \tag{6}$$

Following Prandtl's construction for torsion, we represent the only nonzero shear components by a scalar potential $\Phi=\Phi(r,z)$ as

$$\tau_{r\theta} = \frac{1}{r^2}\Psi_{,z}, \qquad \tau_{z\theta} = -\frac{1}{r^2}\Psi_{,r}. \tag{7}$$

From the axisymmetric kinematics (2) and Hooke's law (4) we have

$$u_{\theta,r} - \frac{u_\theta}{r} = \frac{1}{G}\frac{\Psi_{,z}}{r^2}, \qquad u_{\theta,z} = \frac{1}{G}\frac{\Psi_{,r}}{r^2} \tag{8}$$

Compatibility of mixed derivatives, $u_{\theta,rz} = u_{\theta,zr}$, together with (8) yields after a short calculation

$$\frac{\partial^2\Psi}{\partial r^2}-\frac{3}{r}\frac{\partial\Psi}{\partial r}+\frac{\partial^2\Psi}{\partial z^2}=0,\quad 0\le r\le R(z),\qquad 0\le z\le L. \tag{9}$$

If the lateral surface is traction-free, the shear stress component in the θ-direction projected onto the surface normal must vanish. Geometrically, this means that as you move along the boundary Ψ does not change; hence Ψ is constant on the boundary.

$$\Psi(\mathrm{R(z)},\,z)=0\qquad \text{for all}\quad z\in[0,\,\mathrm{L}], \tag{10}$$

which does not affect stresses because only Ψ-gradients enter $\tau_{r\theta}$, $\tau_{z\theta}$ [4].

Axis regularity: $r\to 0$ Finiteness of $\tau_{z\theta}=-(1/r^2)\cdot\Psi_{,r}$ on the axis requires

$$\Psi_{,r}(0,z)=0, \tag{11}$$

and $\Psi(\cdot,z)$ even in r. This is the standard Saint-Venant regularity for axisymmetric torsion[5].

End faces z=0, L: Saint-Venant "soft" end assumption

In Saint-Venant torsion, warping is assumed free at the ends and end effects are neglected. The corresponding approximation is an axial "soft" Neumann condition

$$\Psi_{,z}(r,0)=\Psi_{,z}(r,L)=0\qquad (0\le r<R(z)), \tag{12}$$

which states that no axial gradient of Φ is enforced at the ends. This is a standard closure when the torsion is controlled by data applied far from the ends.

Load control: twist-controlled vs moment-controlled. Because stress depends only on Φ-gradients, the loading can be enforced through the axis value $\Phi(0,z)$. Two practically important control modes are:

Twist-controlled torsion (prescribed twist rate $\kappa(z)$) If the cross-section at axial station z is circular of radius R(z), the elastic solution for a prismatic slice yields the polar moment of inertia

$$J(z)=\frac{\pi}{2}R(z)^4. \tag{13}$$

Relating torque, twist, and Φ on the axis gives

$$T(z)=GJ(z)\kappa(z)=2\pi G\,\Psi(0,\,z)\qquad\Rightarrow\qquad \Psi(0,\,z)=\frac{J(z)}{2\pi}\kappa(z). \tag{14}$$

This sets the axis gauge consistently with the prescribed twist rate [6].

When the applied torque per station (z)) is known, the same identity gives the axis value directly, this is the Ψ-convention counterpart of the classic relation $T=GJ\kappa$. Note that in the Ψ-convention the torque depends only on the axis value: $T(z)=2\pi G\Psi(0,z)$.

$$\Psi(0,\,z)=\frac{T(z)}{2\pi G},\quad\Rightarrow\qquad T(z)=2\pi G\Psi(0,\,z). \tag{15}$$

NUMERICAL METHOD:

Consider a circular bar whose radius varies smoothly along the axis $z\in[0,L]$ according to a prescribed function $R(z)>0$. To place the problem on a fixed computational strip, we introduce the stretched radial coordinate

$$r=\rho\,R(z),\qquad \rho\in[0,\,1], \tag{16}$$

and define the Prandtl stress function on the mapped domain by

$$\Phi(\rho,\,z)\equiv\Psi(r,\,z)=\Psi(\rho R(z),\,z). \tag{17}$$

Applying the chain rule yields the relations between derivatives of Ψ and Φ:

$$\begin{aligned}&\Psi_r=\frac{1}{R}\Phi_\rho,\qquad \Psi_{rr}=\frac{1}{R^2}\Phi_{\rho\rho},\quad \Psi_z=\Phi_z-\rho\frac{R'}{R}\Phi_\rho,\\ &\Psi_{zz}=\Phi_{zz}-2\rho\frac{R'}{R}\Phi_{\rho z}-\rho\frac{R''}{R}\Phi_\rho+\rho^2\frac{(R')^2}{R^2}\Phi_{\rho\rho},\end{aligned} \tag{18}$$

where $R'=dR/dz$, $R''=d^2R/dz^2$. Throughout, subscripts ρ and z denote partial differentiation with respect to those variables.

Governing equation in the mapped (ρ,z)-domain: For axisymmetric Saint-Venant torsion of a circular cross-section, the Prandtl formulation leads (after mapping) to a linear second-order PDE for $\Phi(\rho,z)$ on the strip $(\rho,z)\in(0,1)\times(0,L)$:

$$A(\rho,\,z)\Phi_{\rho\rho}+B(\rho,\,z)\Phi_{\rho z}+C\,\Phi_{zz}+D(\rho,\,z)\Phi_\rho=0, \tag{19}$$

with coefficients

$$A(\rho,\, z)=\frac{1+(\rho R'(z))^2}{R(z)^2},\qquad B(\rho,\, z)=-2\,\frac{\rho R'(z)}{R(z)},\qquad C=1,\qquad D(\rho,\, z)=\frac{3}{\rho R(z)^2}-\frac{\rho R''(z)}{R(z)}. \tag{20}$$

Note that the material shear modulus G and the prescribed twist rate κ_0 do not appear explicitly in the PDE; they enter through boundary data and the post-processing formulas for torque[7].

The boundary conditions consistent with Saint-Venant's assumptions and the mapping are: Lateral (free) surface ρ=1: a constant-gauge condition for the Prandtl function,

$$\Phi(1,\, z)=0,\qquad 0\le z\le L, \tag{21}$$

which is equivalent to the traction-free boundary in this formulation.

Axis regularity/twist control ρ=0: imposing the sectional twist κ_0 via the classical identity

$$T(z)=2\pi G\,\Phi(0,\, z),\qquad T(z)=G\,J(z)\kappa_0,\qquad J(z)=\frac{\pi}{2}R(z)^4, \tag{22}$$

yields the Dirichlet axis condition

$$\Phi(0,\, z)=\frac{J(z)\kappa_0}{2\pi}=\frac{R(z)^4}{4}\kappa_0,\qquad 0\le z\le L. \tag{23}$$

(In discrete form, axis regularity is enforced by mirroring the first off-axis node, e.g. $\Phi_{1,j}$=$\Phi_{0,j}$.)

Ends z=0,L: Saint-Venant "soft ends" (end effects neglected) correspond to homogeneous Neumann data,

$$\Phi_z(\rho,\, 0)=0,\qquad \Phi_z(\rho,\, L)=0,\qquad 0\le\rho\le 1, \tag{24}$$

which are implemented by first-order copies in the axial direction on the mesh.

Finite-difference discretization (with cross derivative)

Let $\rho_i=i\,H_\rho$ with $H_\rho=1/(N_R-1)$ for $i=0,\ldots,N_R-1$, and $z_j=jH_z$ with $H_z=L/(N_z-1)$ for $j=0,\ldots,N_Z-1$. Using second-order central differences, we approximate the derivatives at interior nodes $(i,j),\ 1\le i\le N_R-2,\quad 1\le j\le N_Z-2$, by

$$\Phi_z(\rho,\, 0)=0,\qquad \Phi_z(\rho,\, L)=0,\qquad 0\le\rho\le 1, \tag{25}$$

$$\begin{aligned}
\Phi_{\rho\rho}\big|_{i,j}&\approx\frac{\Phi_{i+1,j}-2\Phi_{i,j}+\Phi_{i-1,j}}{H_\rho^2},\quad \Phi_{zz}\big|_{i,j}\approx\frac{\Phi_{i,j+1}-2\Phi_{i,j}+\Phi_{i,j-1}}{H_z^2},\\
\Phi_{\rho z}\big|_{i,j}&\approx\frac{\Phi_{i+1,j+1}-2\Phi_{i+1,j-1}-\Phi_{i-1,j+1}+\Phi_{i-1,j-1}}{4H_\rho H_z},\qquad \Phi_{\rho}\big|_{i,j}\approx\frac{\Phi_{i+1,j}-\Phi_{i-1,j}}{2H_\rho},
\end{aligned} \tag{26}$$

with the (locally) frozen coefficients

$$A_{i,j}=A(\rho_i,\, z_j),\quad B_{i,j}=B(\rho_i,\, z_j),\quad C=1,\qquad D_{i,j}=D(\rho_i,\, z_j), \tag{27}$$

the discrete balance at (i,j) can be written in the symmetric point-Jacobi form

$$\left(\frac{2A_{i,j}}{H_\rho^2}+\frac{2C}{H_z^2}\right)\Phi_{i,j}=A_{i,j}\,\frac{\Phi_{i+1,j}+\Phi_{i-1,j}}{H_\rho^2}+C\,\frac{\Phi_{i,j+1}+\Phi_{i,j-1}}{H_z^2}+\frac{B_{i,j}}{4H_\rho H_z}f_{i,j}+\frac{D_{i,j}}{2H_\rho}\left(\Phi_{i+1,j}-\Phi_{i-1,j}\right), \tag{28}$$

where

$$f_{i,j}=\Phi_{i+1,j+1}-\Phi_{i+1,j-1}-\Phi_{i-1,j+1}+\Phi_{i-1,j-1}.$$

This linear system is solved efficiently by SOR (successive over-relaxation) with an empirically chosen relaxation parameter $\omega\in(1,2)$. Neumann end conditions are imposed by copying neighboring interior values in z, the axis condition is Dirichlet (with a mirrored ghost), and the lateral boundary is Dirichlet Φ=0.

Nondimensionalization. To present results in a scale-free form and to stabilize parameter studies, we adopt the following reference scales: Length L (already used in Hz), radius $R0$ (inlet radius), twist $\kappa0$, polar moment $J=(\pi/2)R_0^4$. Prandtl function scale: $\Phi^*=(2\pi\Phi)/(J_0\kappa_0)$.

Define the dimensionless axial coordinate and radius[8]

$$\eta=\frac{z}{L}\in[0,\, L],\qquad \hat{R}(\eta)=\frac{R(z)}{R},$$

so that, for a linear taper, $\hat{R}(\eta)=1+\lambda\eta$, with $\lambda=(R_1-R_0)/R_0$. The boundary conditions become

$$\Phi^*(1,\eta)=0, \qquad \Phi^*(0,\eta)=\frac{J(z)}{J_0}=\hat{R}(\eta)^4, \qquad \frac{\partial\Phi^*}{\partial\eta}(\rho,0)=\frac{\partial\Phi^*}{\partial\eta}(\rho,1)=0. \tag{29}$$

The mapped PDE coefficients A, B, C, D formally retain their expressions when written in terms of the physical z; in practice, the discretization remains identical while output and comparisons are reported in the above nondimensional units.

ANALYSIS OF RESULTS

Using the developed model, the torsional behavior of a circular shaft with a variable diameter along its length was numerically analyzed through the finite-difference method. The geometry was defined such that the radius gradually decreased along the shaft's longitudinal direction, representing a linearly tapered configuration. The computational scheme evaluated the Prandtl stress function field over the normalized radial and axial coordinates for each longitudinal section. This scalar field describes how torsional stresses are distributed inside the shaft at different cross-sections. Boundary conditions were applied consistently with the Saint-Venant torsion theory: the stress potential was set to zero along the free lateral surface, while the axial centerline values were prescribed according to the type of loading applied—either torque-controlled or twist-controlled.

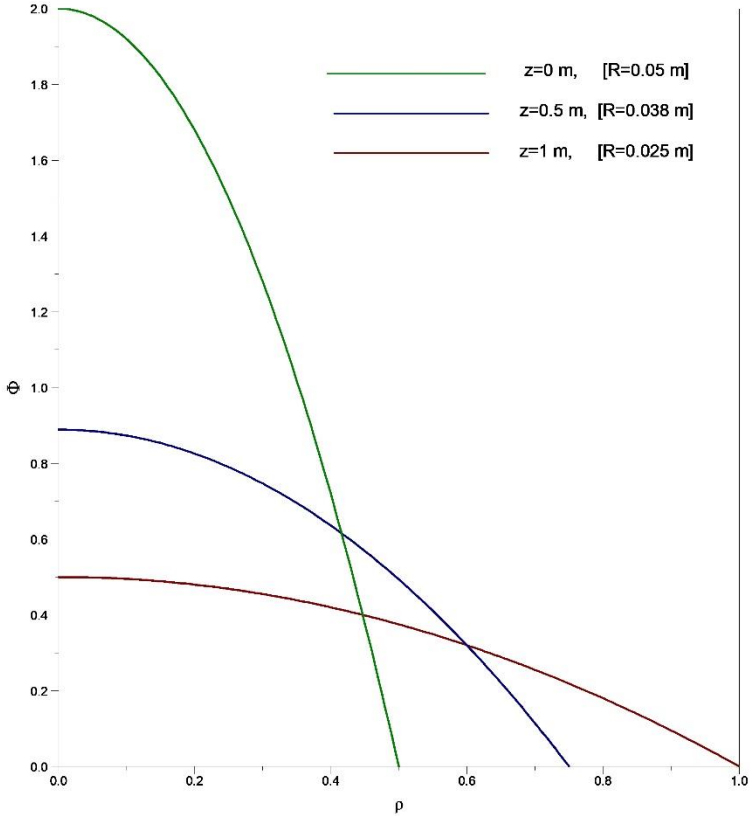

FIGURE 2. Radial profiles of the Prandtl stress function $\Phi(\rho)$ at three axial positions.

The curves correspond to $z=0\,m\,[R=0.05\,m]$, $z=0.5\,m\,[R=0.038\,m]$, and $z=1\,m\,[R=0.025\,m]$. For each section Φ is maximal at the axis and vanishes at the boundary, satisfying $\Phi|\rho=R(z)=0$. As the radius decreases along z, the peak magnitude of Φ drops and the profile becomes flatter, indicating reduced torque capacity and lower shear gradients. The steepest decay is observed at $z=0$, consistent with the largest section radius and the highest polar moment. Consequently, for a fixed applied torque T, the twist rate $\theta'(z)$ must increase as $R(z)$ shrinks to maintain equilibrium. Conversely, if $\theta'(z)$ is prescribed, the transmitted torque decreases roughly with $J(z) \propto R(z)4$, which is consistent with the observed flattening of Φ.

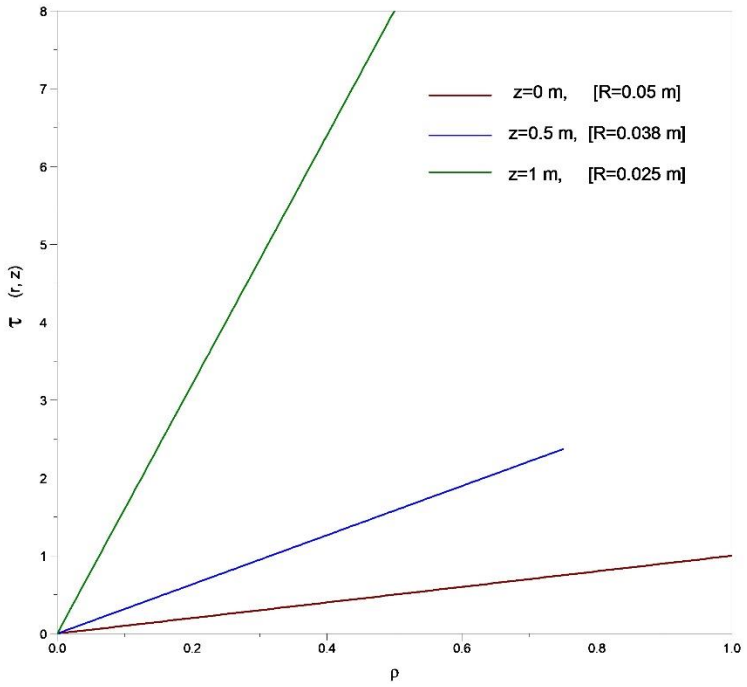

FIGURE 3. Radial shear-stress profiles τ(ρ,z) at three axial positions.

Stress grows linearly with radius and vanishes on the axis, consistent with elastic Saint-Venant torsion $\tau(r,z) \propto r$. The slope increases toward the tip (smaller $R(z)$), so for the same normalized radius ρ the section with the smallest radius carries the highest τ. The maxima occur at the boundaries $\rho = R(z)$, and the strict linearity indicates the response remains in the elastic range without yielding.

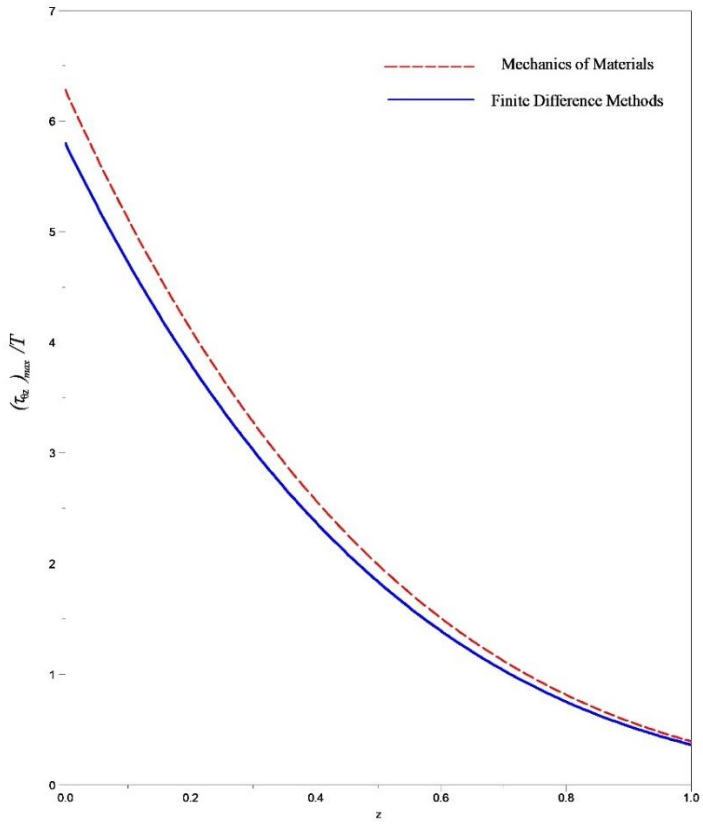

FIGURE 4. Comparison of normalized peak shear vs. axial coordinate.

The plot shows $(\tau_{rz})_{\max}/T$ along the bar for two approaches: a Mechanics-of-Materials (MoM) estimate (dashed red) and the Finite Difference Method (FDM) solution (solid blue). Both curves decrease monotonically with z, reflecting the reduction of section radius and torsional rigidity toward the tip. The MoM curve is slightly higher across the span, indicating a mild overestimation of peak shear when cross-sectional variation is strong. The FDM curve is consistently lower and smoother, capturing geometric taper and boundary effects more accurately.

CONCLUSION

We presented a finite-difference framework for Saint-Venant torsion of circular shafts with axially varying radius, obtained by mapping (r,z) to a fixed (ρ,z) strip and discretizing the resulting elliptic PDE with second-order schemes (with an optional Chebyshev variant in ρ). The method consistently handles twist-controlled and torque-controlled loading through an axis gauge, enforces traction-free lateral boundaries, and is solved efficiently with Successive Over-Relaxation iterations, yielding fields Φ, τ, and the torque profile $T(z)$. Verification against the classical constant-radius solution and section-wise trends confirms accuracy; for tapered geometries the FDM captures the expected decline of Φ and $(\tau_{rz})_{\max}$ toward the tip. Compared with Mechanics-of-Materials estimates, the FDM produces slightly lower, smoother peak-shear predictions in regions of strong radius variation, indicating reduced overestimation by simplified formulas. The framework is immediately extensible to temperature-dependent shear modulus and thermal eigen-twist, making it suitable for design and life assessment of tapered drive shafts, rotors, and industrial rolls.

ACKNOWLEDGMENTS

This study was made possible thanks to budgetary funding from the M.T. Urazbaev Institute of Mechanics and Earthquake Resistance of Structures of the Academy of Sciences of the Republic of Uzbekistan. We express our sincere gratitude to the Academy for its ongoing support and contribution to the advancement of scientific research.

REFERENCES

1. M. H. Sadd, *Elasticity: Theory, Applications, and Numerics* (Elsevier Butterworth–Heinemann, Burlington, 2004), pp 213–229.
2. K. Abdelkader, Z. Toufik and M. B. J. (Ben) Mohamed, Advances in Mechanical Engineering **7(5)**, 1–20 (2015).
3. Y. Shen, Y. Chen, and L. Li, International Journal of Engineering Science, **109**, 14-28 (2016).
4. X.T. Wang, J.B. Li, and H.Y. Ban, Journal of Constructional Steel Research **221**, 111655 (2024).
5. J. E. Turdibekov and F. F. Adilov, "Analysis of elastic prismatic rods subjected to torsional loads," in *International conference: "Ensuring seismic safety and seismic stability of buildings and structures, applied problems of mechanics"*, AIP Conference Proceedings 3265, edited by R. A. Abirov (AIP Publishing, Melville, NY, 2025), pp. 050004, https://doi.org/10.1063/5.0265146.
6. R. A. Abirov, "On the constitutive relations in plasticity at complex loading" In *ASME International Mechanical Engineering Congress and Exposition-2009,* Proceedings **12**, pp. 557–559. https://doi.org/10.1115/IMECE2008-66240
7. F. Adilov, J. Turdibekov and R. Abirov, "On One Approach in Plasticity," in *International conference on actual problems of applied mechanics - Apam-2021* AIP Conference Proceedings 2637, edited by Kh. Khudaynazarov *et al.* (AIP Publishing, Melville, NY, 2022), 030002 https://doi.org/10.1063/5.0119170.
8. F. Moayyedian and J. K. Grabski, Archives of Civil and Mechanical Engineering **21**, 15-17 (2021).
9. A. D. Chernyshev, Journal of Applied Mechanics and Technical Physics **64(6)**, 12-14 (2009).